Title

Surface Charge Effects on Fe(II) Sorption and Oxidation at (110) Goethite Surfaces

Journal

The Journal of Physical Chemistry C, 122(18)

ISSN

1932-7447

Authors

Zarzycki, Piotr

Rosso, Kevin M

Publication Date

2018-05-10

DOI

10.1021/acs.jpcc.8b02099

Surface Charge Effects on Fe(II) Sorption and Oxidation at (110) Goethite Surfaces

Piotr Zarzycki*,† and Kevin M. Rosso‡

†*Energy Geosciences Division, Lawrence Berkeley National Laboratory, 1 Cyclotron Road, Berkeley, CA 94720, United States*

‡*Pacific Northwest National Laboratory, Richland, WA 99352, United States*

E-mail: ppzarzycki@lbl.gov

Phone: (+1) 510 486 6272. Fax: (+1) 510 486 5688

Abstract

Iron(III) oxides and oxyhydroxides are among the most reactive minerals in the environment, with surfaces that become charged when immersed in water. The governing role of surface charge over interfacial processes such as metal sorption is well understood. However, its role in interfacial redox reactions, such as when metal sorption is coupled to interfacial electron transfer, is not. This is mainly because surface charge affects not only the types and densities of surface complexes formed but also their respective driving forces for electron transfer. An important case is Fe(II)-catalyzed recrystallization of Fe(III)-oxyhydroxides, in which Fe(II) sorption and interfacial electron transfer are closely linked.

In this study, we used replica-exchange constant-pH molecular dynamics simulations (Zarzycki, P.; Smith, D. M., Rosso, K. M. *J. Chem. Theory Comput.* **2015**, 11, 1715-1724) to calculate the distance-dependent electrostatic potential at charged (110) surfaces of goethite particles, assessing its effect on previously computed Fe(II) sorption and interfacial electron transfer free energies (Zarzycki, P.; Kerisit, S., Rosso, K. M. *J. Phys. Chem. C* **2015**, 119, 3111-3123). We show that Fe(II) adsorbs preferentially as an inner-sphere complex on the negatively charged surface, and as an outer-sphere complex on the positively charged surface due to both the electrostatic repulsion and high energy barriers that arise from ordered water layers at the interface. The separation distance between adsorbed Fe(II) and the surface largely dictates adiabatic versus nonadiabatic electron transfer regimes for this interface. The findings help unravel the pH-dependence of Fe(II)-catalyzed recrystallization of goethite.

Introduction

Iron oxides and oxyhydroxides are among the most abundant and reactive minerals in the environment.[1,2] When immersed in water, they develop a surface charge due to protonation/deprotonation of surface hydroxyl groups.[1–4] Bulk solution pH is thus an important

master variable controlling the interfacial electrostatics, thermodynamic stability, and sorption of metal ions.

pH-dependent surface charge along with the distribution of solute counter-ions at the interface form an electrical double layer that can span tens of nanometers in thickness.[5–9] However, the specific interactions that enable chemical reactions at the interface, such as electron transfer, operate on a much shorter length-scale, on the order of a few Å, which requires close approach of electron donor/acceptor ions to the surface.[6,8] It is thus clear that to be able to predict whether or not an interface of a metal oxide will react, one needs to understand the balance between electrostatic and chemical forces at the interface.

For Fe(III)-oxides and oxyhydroxides, one of the most challenging examples of pH-dependent interfacial electron transfer chemistry is the recrystallization that occurs autocatalytically when the oxide is in contact with aqueous Fe(II).[10–13] Recently, we have shown by fitting experimental iron isotopic tracer exchange data[11,12] by stochastic simulation that the extent of goethite (α-FeOOH) recrystallization is dictated by the pH-dependent density of Fe(II) adsorbed to the surface, a condition that enables Fe(II) to transfer electrons to goethite Fe(III).[13] Using potential of mean force molecular dynamics simulations, various thermodynamically stable inner and outer-sphere complexes of adsorbed Fe(II) on specific goethite surfaces at charge neutral conditions were identified.[14] What is not yet known is how many of these surface complexes remain stable when the surfaces become charged. Likewise, the corresponding driving force for interfacial electron transfer to the charged surface is not known, although the spontaneous fluctuations of surface potential were shown to play a role.[15] Despite its obvious relevance, the role of pH-dependent surface electrostatics in these kinds of interfacial reactivity topics is, generally, rarely addressed on a molecular-level.

Here, we present replica-exchange constant-pH molecular dynamics simulations of a representative goethite nanoparticle bearing (110) surfaces in water, to compute electrostatic surface potential profiles as a function of surface charge, which then can be translated to their corresponding effects on Fe(II) adsorption and electron transfer across the interface.

To explore non-neutral surface charge while maintaining a neutral simulation cell overall, an imbalance in the proton density across the particle is enforced while allowing full relaxation of surface atoms, water molecules and the equilibrium distribution of surface protons in three dimensions. The goal is to approximate the effect of pH on the previously calculated free energy landscape for Fe(II) adsorption and interfacial electron transfer on the (110) surface in this system.[14] Constant-pH molecular dynamics approach (cpHMD) is a rare event sampling method that allows us to efficiently and simultaneously explore protonation space via Monte Carlo sampling and configuration space via classical molecular dynamics.[15]

Our computational study provides the first molecular level view of how changes in pH may affect Fe(II) sorption and its oxidation by goethite (110) faces, enabling a more robust linkage between molecular simulations and macroscopic observables for the pH-dependence of Fe(II)-catalyzed recrystallization of goethite.

Methods

Although numerous computational methodologies for charged metal oxides have been published (see for instance refs.[16–22]), there are very few atomistic modeling studies that take into account surface proton dynamics explicitly.[18–20,23–29]

A detailed discussion of our constant-pH molecular dynamics algorithm can be found elsewhere.[15] Briefly, our algorithm alternates the Monte Carlo (MC) sampling of the protonation space and molecular dynamics (MD) sampling of configuration space as typically implemented in cpHMD.[30,31] We used the replica-exchange approach to model dynamical proton redistribution.[15] MD simulations for a newly accepted protonation state were carried out for 10 ps with a time step $\delta t = 0.001$ ps, before attempting to change the protonation state via the MC part. A new protonation state is the lowest energy replica among several replicas generated from the current protonation state in the MC protonation step.

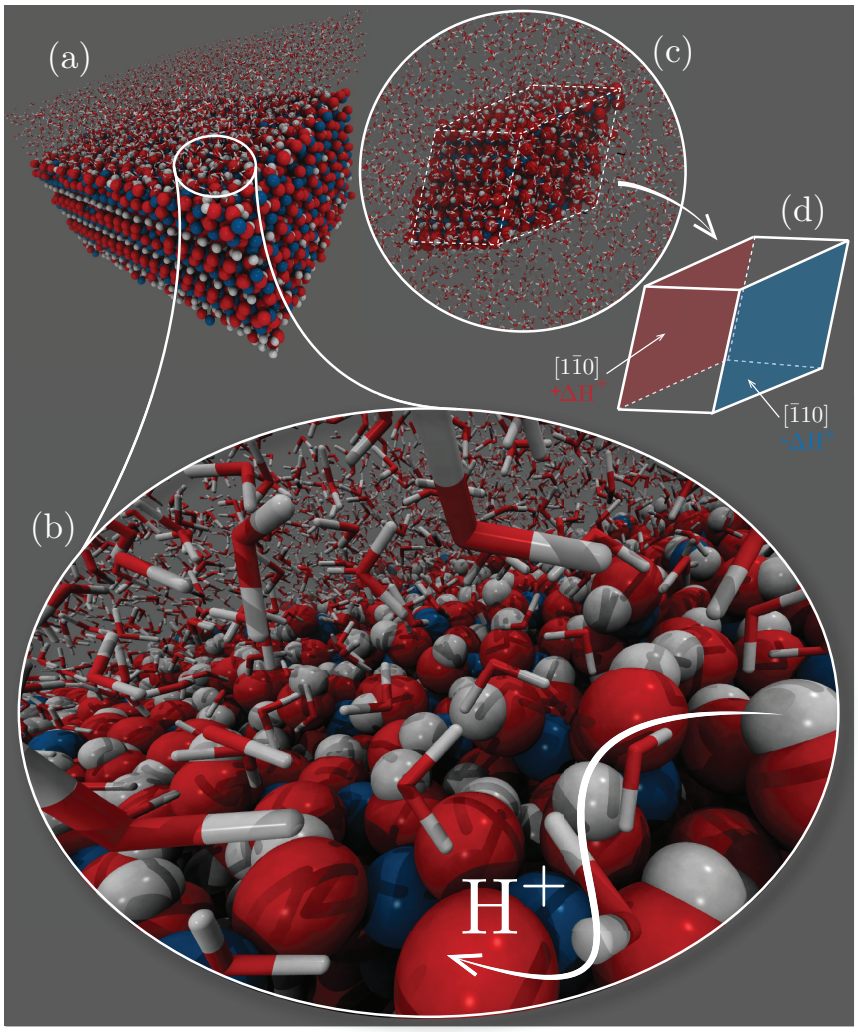

Figure 1: Snapshots of the simulated systems: (a,b) slab geometry of ($\bar{1}$10) goethite crystal faces exposed to the aqueous phase and (c,d) goethite nanoparticle in contact with water. To simulate charged surfaces we imposed a fixed proton imbalance between two mirrored crystal faces ($\bar{1}$10) (i.e., proton excess $+\Delta H^+$ on one face, and a compensating deficiency $-\Delta H^+$ on other face, see panel d). The proton imbalance can be translated into the bulk pH by comparing the simulated and experimental charge densities (see Supporting Information).

Simulation Protocol. We first prepared a goethite nanoparticle that is consistent with prior atom exchange experiments,[10] which principally involve dominant (110) prismatic terminations of needle-shaped crystallites (Pbnm space group notation). To initialize the simulation, we first ensure charge neutrality on any exposed crystal face by protonating all active surface sites in accordance with to their expected proton affinities (i.e., $\sigma_{0(hkl)} = 0$).[32] The goethite and goethite/water interaction parameters were described by the same force-field

as in our previous work.[14,15] After we immersed a charge neutral nanoparticle in a bulk of the SPC/E water molecules,[33,34] we relaxed the initial atomic positions by minimizing configurational energy using the steepest descent algorithm.[35] In the following step, we prepared the charge neutral particle for cpHMD simulations. First, we heated the system to 298 K (Langevin thermostat[36,37] with collision frequency $\gamma = 2$ ps^{-1}, NVT ensemble) for 0.2 ns. Next, we optimized the denisty (i.e., volume of the computational cell) by running NPT molecular dynamics for 4 ns (Berendsen thermostat-barostat[38]). Finally, the cpHMD simulations were carried out for another 30 ns.

The effect of bulk solution pH at various crystal faces was modeled by imposing a fixed protonation imbalance (ΔH^+) between crystallographically equivalent (mirrored) crystal faces. This is accomplished by shifting a number of protons to one crystal face (proton excess, $+\Delta H^+$) at the expense of the proton population at the mirrored crystal face (depleted face, $-\Delta H^+$). This enforced proton disproportion allows us to assess the behavior of positively and negatively charged surfaces in the same simulation, while maintaining nanoparticle (and simulation cell) charge neutrality. By using the available potentiometric titration data[39–41] we can translate ΔH^+ and the surface charge density (σ_0) on a given face to the bulk pH value (see Supporting Information). Our conversion of surface charge to the bulk pH serves only as a first order approximation because reported surface charging curves are sensitive to the experimental conditions (type and concentration of the background electrolyte, temperature, solid loading, particle size/shape and available surface ares).[41]

Surface protons are free to redistribute only within a given crystal face. In other words, they are not allowed to migrate between faces and consequently the magnitude of the proton imbalance is maintained throughout the simulation. This is a major new feature in our constant-pH molecular dynamics model compared to its original implementation[15] in which surface protons were freely redistributed among all exposed crystal faces.

Surface Electrostatics. The charge density, electrostatic field, and potential profiles were obtained directly from the simulation trajectory (see ref.[42–46] for details). The charge density projected onto the y-axis (i.e., normal to surfaces with imposed protonation imbalance) as:

$$\rho(y) = \sum_{i=1}^{N} e q_i \delta(y_i - y) \tag{1}$$

where the sum runs over all atoms in a computational cell (i.e., $i = 1...N$), e is the elementary charge; δ is the Dirac delta function; y_i and q_i are the atom position projected on the y-direction and the partial charge assigned to i-atom, respectively. The electrostatic field and potential are obtained by integrating $\sigma(y)$, that is:

$$E(y) = \int_{y} \rho(y)/\epsilon_0 \, dy \qquad \text{and} \qquad \psi(y) = -\iint_{y} \rho(y)/\epsilon_0 \, dy \tag{2}$$

where ϵ_0 is the vacuum permittivity.

Electrostatic Potential Bias on the Fe(II) Sorption. The adsorption free energy (ΔG) can usually be decomposed into van der Waals and electrostatic contributions ($\Delta G = \Delta G^{vdw} + \Delta G^{elec}$). In the case of Fe(II) ion sorption, the electrostatic contribution to the sorption energy profile along y-direction can be approximated by $2e\psi(y)$.

If the adsorption free energy is known for a charge-neutral surface ($\Delta G(0)$, ΔpH=0), we can scale it to a charged surface by updating the electrostatic contribution, that is:

$$\Delta G(\Delta\text{pH}) = \underbrace{\left[\Delta G(0) - \Delta G^{elect}(0)\right]}_{\Delta G^{vdw}} + \Delta G^{elec}(\Delta\text{pH}) \tag{3}$$

The Fe(II)-adsorption free energies for the neutral (110) goethite surface were taken from our previous work.[14] This energy profile was obtained by calculating the potential of mean force exerted by the oxide surface and water molecules on the hexaquo Fe^{2+} cation as it gradually approached goethite surface.[14] The hexaquo species is the dominant Fe(II) species

in solution over most of the pH range of interest to this study (see Supporting Information), and thus its hydrolysis species were not necessary to explicitly treat in the simulations. The ensemble average of forces acting on the ion in the direction normal to the surface was integrated at each distance (i.e., partially constrained dynamics) to obtain the adsorption free energy (i.e., $\Delta G(y^*) = -\int_{\infty}^{y^*} \langle f_y \rangle dy$).[14]

Electrostatic Potential Bias on the Interfacial Electron Transfer. The rate of electron transfer from an inner-sphere adsorbed Fe(II) to Fe(III) at the oxide surface is given by the adiabatic formula:[14,47]

$$k_{ET} = \kappa\nu \exp\left[-\frac{1}{k_B T}\left(\frac{(\Delta G_{ET} + \lambda)^2}{4\lambda} - V_{AB}\right)\right] \tag{4}$$

where ν is a frequency of vibrational mode acting along the nuclear reaction coordinate, λ is the reorganization energy, ΔG_{ET} is the electron transfer free energy, V_{AB} is an electronic coupling matrix element between reactants and products wave functions. The rate of electron transfer from an outer-spherically adsorbed Fe(II) to oxide surface is quantified by a non-adiabatic expression (high-temperature limit):[14,47,48]

$$k_{ET} = \frac{2\pi}{\hbar}\frac{|V_{AB}|^2}{\sqrt{4\pi\lambda k_B T}} \exp\left[-\frac{(\Delta G_{ET} + \lambda)^2}{4\lambda k_B T}\right] \tag{5}$$

where κ is the adiabaticity factor and $\hbar = h/2\pi$ is the reduced Planck constant. A detailed discussion of ET-parameters can be found elsewhere.[14,47–50]

ΔG_{ET} can also be decomposed into van der Waals and electrostatic contributions. The electrostatic part can be approximated by: $\Delta G_{ET}^{elec} = -e\left(\psi(y) - \psi(0)\right)$ (y is the distance of sorbed Fe(II) from the surface). The electron transfer free energy obtained for a charged neutral surface ($\Delta G_{ET}(0)$) can be scaled to a charged surface ($\Delta G_{ET}(\Delta pH)$) as follows:

$$\Delta G_{ET}(\Delta pH) = \underbrace{\Delta G_{ET}(0) - \Delta G_{ET}^{elect}(0)}_{\Delta G_{ET}^{vdw}} + \Delta G^{elec}(\Delta pH) \tag{6}$$

The free energy and solvent reorganization energies for electron transfer from Fe(II) adsorbed as inner-sphere, or outer-sphere complexes on goethite (110) surfaces were taken from our previous study.[14] These energies were obtained by calculating the adiabatic free energy profiles (Marcus' parabolas[51]) by using the umbrella sampling method developed by Warshel and co-workers.[52–54] In a number of the umbrella windows, the force-field parameters for the adsorbed Fe(II) and surface Fe(III) were morphed into each other using a linear coupling scheme.[14] Next, the ensemble averages of the energy gap from each window were used to construct the electron transfer free energy parabola.[14,52–55]

Results and Discussion

The primary goal of our simulations was to assess the effects of nonzero surface charge on Fe(II) adsorption energetics and the kinetics of the interfacial electron transfer to Fe(III) in the (110) goethite surface. Our model should help unravel coupled effects that occur during Fe(II)-catalyzed goethite recrystallization at different solution conditions by quantifying how pH affects both Fe(II) adsorption and electron transfer rates from energetically accessible surface complex geometries.

Imposed Surface Potential Gradient Across the Goethite Particle. In Figure 2a,b we show electrostatic potential profiles projected onto the axis normal (y) for the proton-enriched and proton-depleted (110) crystal faces (see Fig. 1c,d). In Figure 2a we showed the electrostatic potential calculated for a probe charge approaching the positively charged face, whereas in Figure 2b we show the same for the negatively charged face. The difference in protonation of two mirrored faces results in a potential gradient across the cell ($\Delta\psi$) which, in addition to its contribution to the interfacial electron transfer free from an adsorbed donor such as Fe(II), may may also act as a driving force for transfer of donated charge through the goethite nanoparticle (as electron or hole carriers) between these faces - this aspect was examined in our previous work in terms of spontaneous potential gradients due to proton

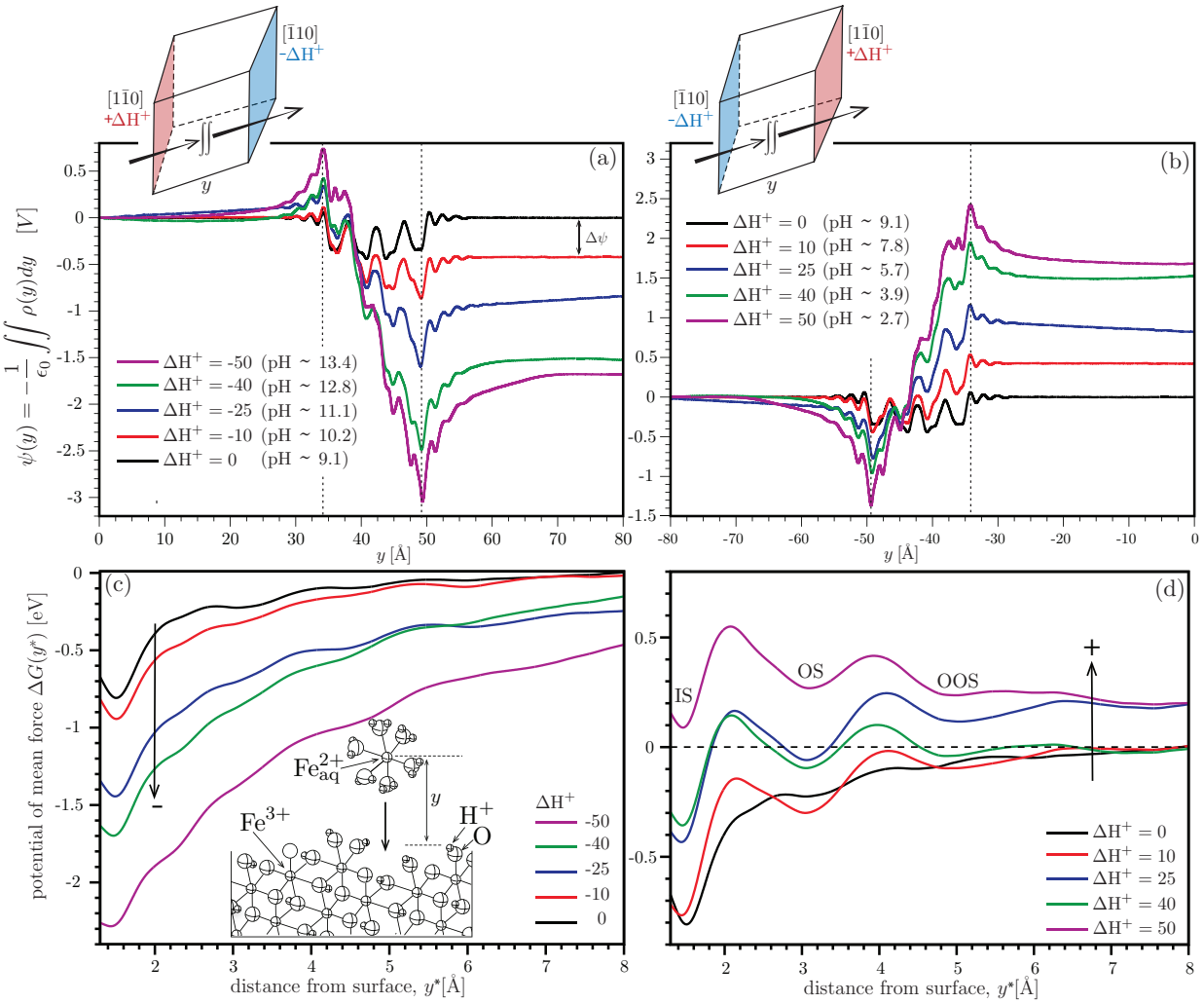

Figure 2: Electrostatic potential profiles $\psi(y)$ calculated using a probe point charge approaching the positive (a, $\Delta H^+ > 0$) and negative (b, $\Delta H^+ < 0$) crystal faces. The electrostatic gradient ($\Delta\psi$) across the particle is due to a fixed H^+ excess ($\Delta H^+ > 0$) on one crystal face at the expense of H^+ population on the mirrored one ($\Delta H^+ < 0$). In panel (c,d) we show the corresponding effect of the electrostatic potential ($\psi(y^*)$) on the Fe(II) adsorption free energy. The potential calculated for particle (a,b) is applied to the Fe(II) adsorption free energy obtained for ($\bar{1}10$) crystal face from our previous work.[14] We used two distance parameters: y-coordinate of the computational cell and y^* is the distance from the ($\bar{1}10$) surface.

fluctuations.[15]

Firstly, from the results it can be observed that the voltage drop between the H^+-imbalanced faces increases with increasing ΔH^+ (Fig. 2a,b). Because the proton imbalance is fixed, the calculated potential jumps across the particle ($0.52\ \text{V} \leq \Delta\psi \leq 2\ \text{V}$) are much

larger than expected for a system near equilibrium (see our previous report: $\Delta\psi \sim k_B T$ (26 meV)[15]). These rather large gradients are nonetheless useful for establishing trends in the surface potential effect. The bulk pH values corresponding to the imposed ΔH^+ can be estimated by comparing the surface charge density in the simulations with potentiometric titration data[39–41] (see Supporting Information and Tables 1,2). For the maximum ΔH^+, the corresponding bulk solution values are ∼13 for the negatively charged face (proton deficient) and ∼3 for the positively charged face (proton enriched). Lower values of ΔH^+ systematically reach into less extreme pH values. From this calibration of our simulation data to measured surface charge densities we estimate the point of zero charge (PZC) to be approximately at pH 9.1 (See Supporting Information).

Effects of Surface Potential on Fe(II) Adsorption. In Figure 2c,d the Fe(II) adsorption free energy is shown for neutral (black line, results taken from our previous study[14]), negatively charged (Fig. 2c) and positively charged (Fig. 2d) (110) surfaces. The free energy profiles from our previous work were computed using the hexaquo Fe(II) aqueous complex, which is the primary Fe(II) species over the pH range from 0 to 9.5 according to well established equilibrium thermodynamics data (see Supporting Information). At higher pH values the hydrolysis species of Fe(II) become dominant and the system is unstable with respect to precipitation of reduced or mixed-valent iron oxides.[1] These well-known experimental facts mean that while we explicitly calculate the effect of the bulk solution pH on the surface charge we do not have to likewise explicitly treat the speciation of Fe(II) and can restrict our analysis to the hexaquo cation because of its wide stability range. Hence, although higher effective solution pH values were explored the actual pH range that the present calculations strictly apply to is pH 0 to 9.5.

As expected, with increasingly larger negative (positive) surface charge Fe(II) is more strongly electrostatically attracted to (repelled from) the surface. In the case of the charge-neutral surface, as shown in our previous work the adsorption free energy profile shows

a subtle barrier between inner- and outer-sphere Fe(II)-complexes,[14] which gradually disappears with increasing the negative surface charge. In the extreme hypothetical case of ΔH^{+}=50 (pH > 13, see Table 1) we obtain almost a linear relationship between adsorption free energy and Fe(II) distance from the surface (Fig. 2c).

This suggests that for neutral to negatively charged goethite surfaces, which would be relevant only above pH∼9, Fe(II) adsorption would be dominated by inner-sphere complexes, and interfacial electron transfer kinetics would lie within the adiabatic regime (cf.[14]). Hence, for a negatively charged goethite surface, which again remains mostly beyond the relevant stability range of aqueous Fe(II) ions, interfacial electron transfer would be facile.

In contrast, the positively charged surface decreases inner-sphere Fe(II) adsorption both by providing additional electrostatic repulsion for an approaching Fe(II) but also by increasing the magnitude of the free energy barriers for forming surface complexes (Fig. 2d). In particular, the calculations predict that even for a weakly positive surface charge the free energy barriers between inner- (IS) and outer-sphere (OS) Fe-coordination become more pronounced, with the appearance of additional energy well far from the surface (here referred as outer-outer-sphere complex, OOS). The calculated height of these barriers (Table 1) is typically above the available thermal energy (kT) at room temperature, increasing systematically as bulk solution pH decreases. Their position is dictated by the position of interfacial water layers,[14] which suggests that the energy penalty arises from the strain energy for the hydrated Fe(II) ion to penetrate the semi-rigid interfacial water layers as it approaches the surface. It is a manifestation of the hydration forces due to solvent layering.[56–58] Collectively, this picture is the molecular level explanation for the rapidly diminishing net sorption of Fe(II) to goethite surface below the PZC that ceases to amounts below detection by bulk pH values lower than 4.[39–41]

The outer-sphere Fe(II)-adsorption minima arise when water in Fe(II) first solvation sphere fits well into the structure of the hydrogen-bonded network of the interfacial hydration layers, whereas the barriers arise when there is a large mismatch. The Fe(II)-surface distances

for IS and OOS vary only slightly among all cases, which confirms that these positions are dictated by the interfacial water layers, whose positions are relatively insensitive to pH.

Interestingly, for weakly positive surface charge exergonic free energy minima for Fe(II) adsorption still exist. The minima between barriers are low enough to trap Fe(II) ions near the surface. However, the barriers to arrive at these states are high enough to maintain kinetically limited direct access of Fe(II) to the surface (Table 1). In particular, for pH $<$ PZC ($\Delta H^+ > 0$) the energy barrier between the inner- and outer-sphere geometries is greater than 6 kT. Hence, Fe(II) is unlikely to reach the inner-sphere geometry - a distance required for fast interfacial electron transfer in the adiabatic regime. Instead, the electron transfer from Fe(II) in OS or OOS locations must occur over a relatively large donor-acceptor distance entailing what would necessarily be orders of magnitude slower rates. For such long-distances, it is expected that electron transfer would be in the nonadiabatic regime (cf.[14]).

Table 1: Energy barriers for transitions from outer-sphere to inner-sphere (OS→IS) and outer-outer-sphere to outer-sphere (OOS→OS) complex geometries of adsorbed Fe(II) ion at pH above PZC (in kT units).

ΔH^+	pH	$\Delta G_{barrier}$ [kT] (OS → IS)	$\Delta G_{barrier}$ [kT] (OOS → OS)
10	7.8 ± 1.0	6.17	3.09
25	5.7 ± 1.0	8.72	4.96
40	3.9 ± 1.3	9.39	5.50
50	2.7 ± 1.5	10.87	6.84

Effect of surface potential on the electron transfer free energy. In Figure 3a we show a diagram of electron transfer free energy parabolas (see Marcus theory[51,59]). In Figure 3b,c we show calculated electron transfer free energy surfaces that take into account varying surface charge (σ_0, ΔH^+). These are obtained by adjusting previous results from molecular dynamics simulations[14] for the effect of surface electrostatic potential by scaling the free energy according to eq. (6). In Table 2 we list corresponding electron transfer rates for inner- and outer-sphere complexes as a function of bulk phase pH.

The electrostatic potential bias has a stronger influence on the outer-sphere Fe(II) to

Table 2: pH-dependent electron transfer rates for inner-sphere complex geometry (adiabatic ET, $k_{ET(IS)}$) and outer-sphere surface complex geometries (nonadiabatic ET, $k_{ET(OS)}$). The values of the bulk pH are approximated by comparing the surface charge density (σ_0) of a simulated particle with the potentiometric titration data[39–41] (see Supporting Information).

ΔH^+	σ_0 [C/m^2]	pH	$k_{ET(IS)}$ [1/s]	$k_{ET(OS)}$ [1/s]
50	0.353	2.7 ± 1.5	127	1.83E-03
40	0.282	3.9 ± 1.3	20.8	1.19E-04
25	0.176	5.7 ± 1.0	7.38	1.33E-05
10	0.071	7.8 ± 1.0	2.01	1.20E-06
0	0.00[a]	9.1 ± 1.0	1.96E-02	1.75E-09
-10	-0.071	10.2 ± 0.9	9.53E-04	3.90E-11
-25	-0.176	11.1 ± 1.3	1.68E-04	1.19E-12
-40	-0.282	12.8 ± 0.8	2.71E-05	5.07E-14
-50	-0.353	13.4 ± 0.7	2.04E-06	1.08E-15

[a]Point of Zero Charge (PZC)

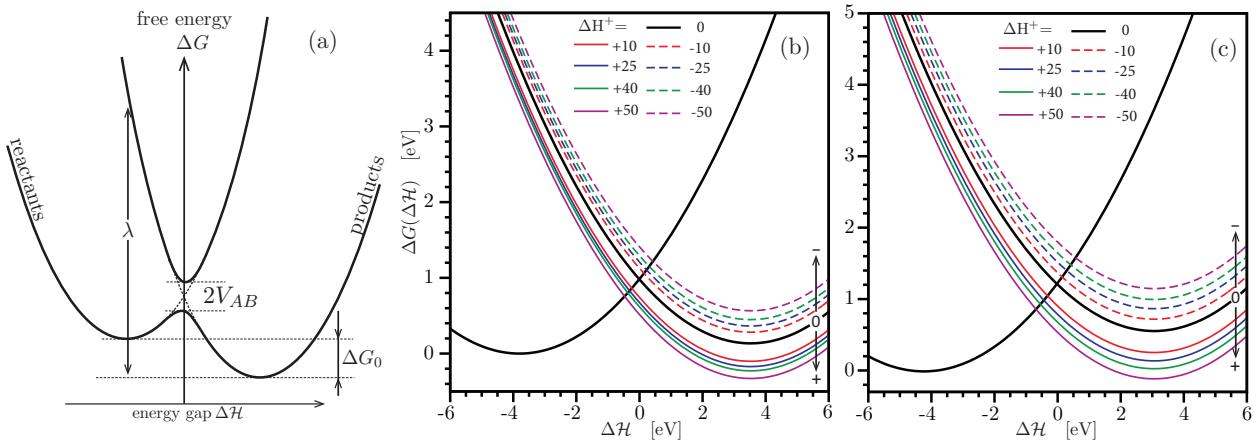

Figure 3: Schematic representation of the parabolic electron transfer potential energy surfaces (a). According to the Marcus' model, the electron transfer rate depends on the reorganization energy (λ), energy barrier (ΔG_0), and electronic coupling (V_{AB}), see eqs. (4,5). In panel (b,c) we show the potential energy surfaces for electron transfer between Fe(II) in the inner-sphere (b) and outer-sphere (c) complex geometry and the nearest surface Fe(III) ion for various protonation state of the surface (i.e., $\Delta H^+ > 0$ positive surface charge, $\Delta H^+ = 0$ neutral surface, and $\Delta H^+ < 0$ is negatively charged surface). The potential energy surfaces for the neutral α-FeOOH taken from our previously reported simulations.[14]

surface Fe(III) electron transfer energetics than the inner-sphere ones. This is because the magnitude of the potential bias increases with a donor-acceptor separation (see Fig. 2a,b). There is also an additional effect from the fact that an electron is repelled by the negatively

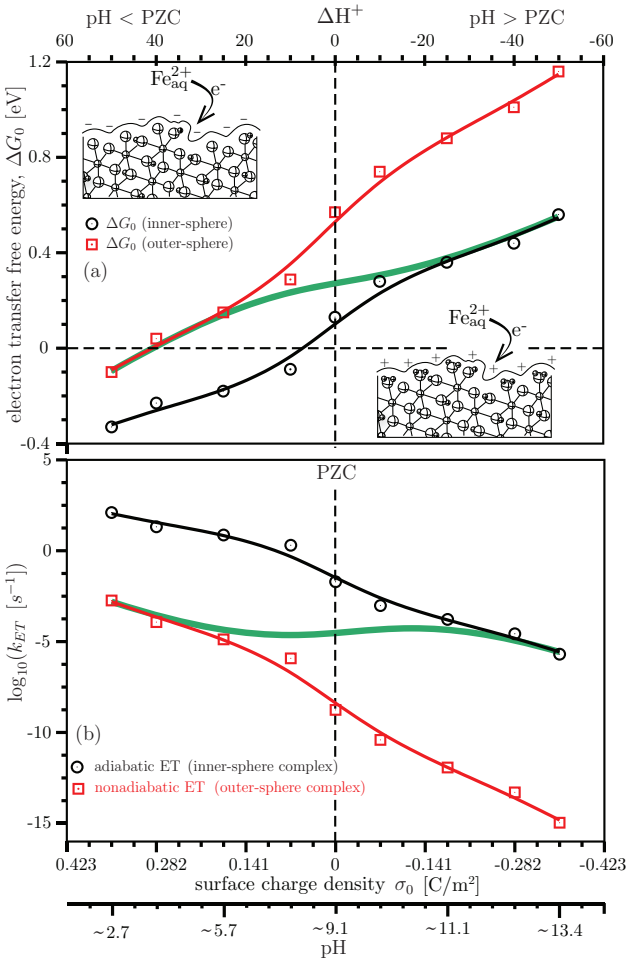

Figure 4: Net effect of surface protonation state on the free energy of electron transfer between Fe(II) in the inner-sphere and outer-sphere complex geometry and the nearest surface Fe(III) of the (110) crystal face of α-FeOOH. In panel b, we show corresponding electron transfer rates (ΔG taken from panel a, values of other parameters in eqs. (4,5) are taken from ref.[14]). The green lines represent hypothetical electron transfer free energy (a) and rate constant (b) that could be observed experimentally (macroscopic, ensemble averaged). The values for the charge-neutral case (ΔH^+=0) are taken from our previous simulations.[14] The values ΔH^+ and σ_0 on the x-axis are taken from our simulation study, whereas the pH scale is an approximation based on the experimental titration data (see Supporting Information).

charged surface and attracted by positively charged one - as indicated by the vertical shift in ΔG (products branch, Fig. 3b,c). This trend is the inverse of and opposes the surface charge effect on Fe(II) ion adsorption, thus complicating interpretation of the ability of goethite (110) surface to bind and oxidize Fe(II) at various pH values.

In an attempt to place all synergistic and competing effects on the same scale and predict

the net outcome, in Fig. 4 we show the calculated electron transfer free energies ΔG_0 (Fig. 4a) and estimated rates (Fig. 4b) as a function of the bulk pH for the inner- and outer-sphere sorbed Fe(II). The sign of ΔG is given in the usual sense (>0 means electron transfer is endergonic, whereas $\Delta G < 0$ is exergonic). As shown in Fig. 4a the outer-sphere ET is less plausible than inner-sphere ET for all ΔH^+ values, consistent with the expectation for charge-neutral surfaces.[14] However, we also need to take into account that at pH < PZC outer-sphere complexes are much more likely than the inner-sphere complexes, and vice versa at pH>PZC. This means that at low pH an interfacial electron transfer would have to be mediated primarily by outer-sphere complexes, whereas at high pH electron transfer would primarily be mediated by inner-sphere complexes. The net behavior for elementary interfacial electron transfer steps as a function of pH should thus be well approximated by the trends shown in green lines in Figure 4.

One interesting result of this analysis is that net interfacial electron transfer rate per adsorbed Fe(II) becomes approximately independent of pH (Fig. 4b). Our simulation study suggests that electron transfer occurs via the inner-sphere geometry in the adiabatic regime at pH > PZC (eq. (4)) and via the outer-sphere Fe(II) geometry in the nonadiabatic regime at pH < PZC (eq. (5)). In Fig. 4b we show an estimated electron transfer rate in adiabatic and nonadiabatic regimes for the inner- and outer-spherically adsorbed Fe(II) on the (110) goethite face. Despite the different mathematical formalisms, the values of the adiabatic rate constant at high pH are similar to the nonadiabatic rate constant at low pH. One can expect that as pH increases from the low to high values, the electron transfer rate should smoothly move from nonadiabatic (pH<PZC) to adiabatic (pH>PZC) regime (green line in Fig. 4b). The experimental rate constant corresponds to the ensemble-averaged electron transfer rate, with pH-dependent contribution from both inner- and outer-sphere Fe(II)-configurations. An analogous, smooth transition is expected on the macroscopic electron transfer free energy (green line in Fig. 4a). The microscopic experimentally observable rate thus depends more on the density of adsorbed Fe(II), which varies strongly with pH, rather than the interfacial

electron transfer rate per Fe(II).

Hence, even at low pH the interfacial ET process is kinetically feasible. However, the net flux of these steps would be severely limited by a very low density adsorbed Fe(II), taking the form of dilute outer-sphere complexes. In this pH range, our simulations suggest a large energy barrier between inner- and outer-sphere complexes that would preclude inner-sphere complex formation. However, this does not exclude the possibility of Fe(II) oxidation from outer-sphere complexes, followed by precipitation of product (Fe(III) cations) onto the surface, possibly driven by structured water molecules at the interface expelling Fe(III) from their layers. This is fully consistent with experimental sorption studies[8] showing that Fe(II) sorption can occur well below the PZC. Furthermore, isotope-tracer experiments have also shown Fe(II)-catalyzed isotopic exchange at pH 5.0, suggesting feasible adsorption and interfacial electron transfer from aqueous Fe(II) at low pH.[11]

Conclusions

Using replica-exchange constant-pH molecular dynamics we calculated the distance-dependent electrostatic potential at charged (110) goethite particle surfaces as a function of bulk solution pH, and then used this potential to estimate the energetics of sorption and interfacial electron transfer of aqueous Fe(II) ions. We found that Fe(II) adsorbs preferentially in an inner-sphere complex geometry above the PZC on the negatively charged surface, and in an outer-sphere or outer-outer-sphere complex geometry below the PZC on the positively-charged surface. The sorption geometry dictates the separation distance for electron exchange across the interface, which in turn determines adiabaticity. The position of free energy barriers correlates well with the position of semi-rigid water layers, a manifestation of hydration forces in determining the charge distribution at iron oxide/electrolyte interfaces. However, the height of the energy barriers between various surface complexes is primarily dictated by the electrostatics.

Based on our simulation results we propose that the electron transfer mechanism switches from the nonadiabatic regime at pH<PZC to the adiabatic regime at pH>PZC, which results in a smooth conversion of energetics and rates per adsorbed Fe(II) as a function of pH. The pH-triggered change in mode of Fe(II) sorption while maintaining a relatively pH-independent interfacial electron transfer rate suggests that the overall pH dependence of Fe(II)-catalyzed recrystallization of goethite originates primarily from the sorption density of Fe(II).[10,11] Our findings are important because a similar interplay between surface charge and interfacial reactivity should operate in other metal oxide/aqueous interfacial geochemical processes involving redox-active metal oxide minerals.

Acknowledgement

This material is based upon work supported by the U.S. Department of Energy (DOE), Office of Science, Office of Basic Energy Sciences, Chemical Sciences, Geosciences, and Biosciences Division through its Geosciences program at the Pacific Northwest National Laboratory (PNNL). A portion of this research was performed using EMSL, a national scientific user facility sponsored by the DOE's Office of Biological and Environmental Research and located at Pacific Northwest National Laboratory. Pacific Northwest National Laboratory (PNNL) is a multiprogram national laboratory operated for DOE by Battelle. P.Z. also acknowledges support from U.S. Department of Energy (DOE) Chemical Sciences, Geosciences, and Biosciences Division under Contract DE-AC02-05CH11231.

Supporting Information Available

The correspondence between ΔH^+ and bulk pH based on the potentiometric titration data reported for goethite particles.[39–41] The calculations of the pH-dependent Fe(II) aqueous speciation under redox-inert conditions using PHREEQC.[60]

References

(1) Cornell, R. M.; Schwertmann, U. *The Iron Oxide. Structure, Properties, Reactions, Occurrence and Uses*; Wiley: Weinheim, 2003.

(2) Brown, G. E.; Henrich, V. E.; Casey, W. H.; Clark, D. L.; Eggleston, C.; Felmy, A.; Goodman, D. W.; Grätzel, M.; Maciel, G.; McCarthy, M. I. et al. Metal Oxide Surfaces and Their Interactions with Aqueous Solutions and Microbial Organisms. *Chem. Rev.* **1999**, *99*, 77–174.

(3) Hiemstra, T.; Venema, P.; van Riemsdijk, W. Intrinsic Proton Affinity of Reactive Surface Groups of Metal (Hydr)oxides: The Bond Valence Principle. *J. Colloid Interface Sci.* **1996**, *184*, 680–692.

(4) Hiemstra, T.; van Riemsdijk, W. H. Effect of Different Crystal Faces on Experimental Interaction Force and Aggregation of Hematite. *Langmuir* **1999**, *15*, 8045–8051.

(5) Lyklema, J. *Fundamentals of Interface and Colloid Surface*; Academic Press: San Diego, 2001; Vol. 2: Solid-Liquid Interfaces.

(6) Dzombak, D. and Morel, F. M. M., *Surface Complexation Modeling: Hydrous Ferric Oxide*; Wiley: New York, 1990.

(7) Kosmulski, M. *Surface Charging and Points of Zero Charge*; CRC Press: Boca Raton, 2009.

(8) Hiemstra, T.; van Riemsdijk, W. H. Adsorption and Surface Oxidation of Fe(II) on Metal (Hydr)Oxides. *Geochim. Cosmochim Acta* **2007**, *71*, 5913–5933.

(9) Bradl, H. B. Adsorption of Heavy Metal Ions on Soils and Soils Constituents. *J. Colloid Interface Sci.* **2004**, *277*, 1–18.

(10) Handler, R. M.; Beard, B. L.; Johnson, C. M.; Scherer, M. M. Atom Exchange between Aqueous Fe(II) and Goethite: An Fe Isotope Tracer Study. *Environ. Sci. Technol.* **2009**, *43*, 1102–1107.

(11) Handler, R. M.; Frierdich, A. J.; Johnson, C. M.; Rosso, K. M.; Beard, B. L.; Wang, C.; Latta, D. E.; Neumann, A.; Pasakarnis, T.; Premaratne, W. A. P. J. et al. Fe(II)-Catalyzed Recrystallization of Goethite Revisited. *Environ. Sci. Tech.* **2014**, *48*, 11302–11311.

(12) Joshi, P.; Gorski, C. A. Anisotropic Morphological Changes in Goethite during Fe^{2+}-Catalyzed Recrystallization. *Environ. Sci. Technol.* **2016**, *50*, 7315–7324.

(13) Zarzycki, P.; Rosso, K. M. Stochastic Simulation of Isotopic Exchange Mechanisms for Fe(II)-Catalyzed Recrystallization of Goethite. *Environ. Sci. Technol.* **2017**, *51*, 7552–7559.

(14) Zarzycki, P.; Kerisit, S.; Rosso, K. M. Molecular Dynamics Study of Fe(II) Adsorption, Electron Exchange, and Mobility at Goethite (α-FeOOH) Surfaces. *J. Phys. Chem. C* **2015**, *119*, 3111–3123.

(15) Zarzycki, P.; Smith, D. M.; Rosso, K. M. Proton Dynamics on Goethite Nanoparticles and Coupling to Electron Transport. *J. Chem. Theory Comput.* **2015**, *11*, 1715–1724.

(16) Borkovec, M. Origin of 1-pK and 2-pK Models for Ionizable Water-Solid Interfaces. *Langmuir* **1997**, *13*, 2608–2613.

(17) Kerisit, S.; Rosso, K. M. Computer Simulation of Electron Transfer at Hematite Surfaces. *Geochim. Cosmochim. Acta* **2006**, *70*, 1888–1903.

(18) Rustad, J. R.; Hay, B. P. A Molecular Dynamics Study of Solvated Orthosilicic Acid and Orthosilicate Anion Using Parametrized Potentials. *Geochim. Cosmochim. Acta* **1995**, *59*, 1251–1257.

(19) Rustad, J. R.; Wasserman, E.; Felmy, A. R.; Wilke, C. Molecular Dynamics Study of Proton Binding to Silica Surfaces. *J. Colloid Interface Sci.* **1997**, *198*, 119–129.

(20) Rustad, J. R.; Felmy, A. R. The Influence of Edge Sites on the Development of Surface Charge on Goethite Nanoparticles: A Molecular Dynamics Investigation. *Geochim. Cosmochim. Acta* **2005**, *69*, 1405–1411.

(21) Kerisit, S. Water Structure at Hematite–Water Interfaces. *Geochim. Cosmochim. Acta* **2011**, *75*, 2043–2061.

(22) Halley, J. W.; Rustad, J. R.; Rahman, A. A Polarizable, Dissociating Molecular Dynamics Model for Liquid Water. *J. Chem. Phys.* **1993**, *98*, 4110.

(23) Zarzycki, P. Comparison of the Monte Carlo Estimation of Surface Electrostatic Potential at the Hematite (0001)/Electrolyte Interface with the Experiment. *Appl. Surf. Sci.* **2007**, *253*, 7604–7612.

(24) Zarzycki, P.; Rosso, K. M. Nonlinear Response of the Surface Electrostatic Potential Formed at Metal Oxide/Electrolyte Interfaces. A Monte Carlo Simulation Study. *J. Colloid Interface Sci.* **2010**, *341*, 143–152.

(25) Zarzycki, P.; Chatman, S.; Preočanin, T.; Rosso, K. M. Electrostatic Potential of Specific Mineral Faces. *Langmuir* **2011**, *27*, 7986–7990.

(26) Tocci, G.; Michaelides, A. Solvent-Induced Proton Hopping at a Water–Oxide Interface. *J. Phys. Chem. Lett.* **2014**, 474–480.

(27) Gaigeot, M.-P.; Sprik, M.; Sulpizi, M. Oxide/water Interfaces: How the Surface Chemistry Modifies Interfacial Water Properties. *J. Phys.: Condens. Matter* **2012**, *24*, 124106.

(28) Tazi, S.; Rotenberg, B.; Salanne, M.; Sprik, M.; Sulpizi, M. Absolute Acidity of Clay Edge Sites from Ab-initio Simulations. *Geochim. Cosmochim. Acta* **2012**, *94*, 1–11.

(29) Liu, X.; Lu, X.; Sprik, M.; Cheng, J.; Meijer, E. J.; Wang, R. Acidity of Edge Surface Sites of Montmorillonite and Kaolinite. *Geochim. Cosmochim. Acta* **2013**, *117*, 180–190.

(30) Mongan, J.; Case, D. A.; McCammon, J. A. Constant pH Molecular Dynamics in Generalized Born Implicit Solvent. *J. Comput. Chem.* **2004**, *25*, 2038–2048.

(31) Mongan, J.; Case, D. A. Biomolecular Simulations at Constant pH. *Curr. Opin. Struct. Biol.* **2005**, *15*, 157–163.

(32) Venema, P.; Hiemstra, T.; Weidler, P. G.; van Riemsdijk, W. H. Intrinsic Proton Affinity of Reactive Surface Groups of Metal (Hydr)oxides: Application to Iron (Hydr)oxides. *J. Colloid Interface Sci.* **1997**, *198*, 282–295.

(33) Berendsen, H. J. C.; Grigera, J. R.; Straatsma, T. P. The Missing Term in Effective Pair Potentials. *J. Phys. Chem.* **1987**, *91*, 6269–6271.

(34) Kusalik, P. G.; Svishchev, I. M. The Spatial Structure in Liquid Water. *Science* **1994**, *265*, 1219–1221.

(35) Press, W. H.; Teukolsky, S. A.; Vetterling, W. T.; Flannery, B. P. *Numerical Recipes. The Art of Scientific Computing*, 3rd ed.; Cambridge University Press: Cambridge, 2007.

(36) Pastor, R. W.; Brooks, B. R.; Szabo, A. An Analysis of the Accuracy of Langevin and Molecular Dynamics Algorithms. *Mol. Phys.* **1988**, *65*, 1409–1419.

(37) Uberuaga, B. P.; Anghel, M.; Voter, A. F. Synchronization of Trajectories in Canonical Molecular-Dynamics Simulations: Observation, Explanation, and Exploitation. *J. Chem. Phys.* **2004**, *120*, 6363–6374.

(38) Berendsen, H. J. C.; Postma, J. P. M.; van Gunsteren, W. F.; DiNola, A.; Haak, J. R.

Molecular Dynamics with Coupling to an External Bath. *J. Chem. Phys.* **1984**, *81*, 3684–3690.

(39) van Geen, A.; Robertson, A. P.; Leckie, J. O. Complexation of Carbonate Species at the Goethite Surface: Implications for Adsorption of Metal Ions in Natural Waters. *Geochim. Cosmochim. Acta* **1994**, *58*, 2073–2086.

(40) Gaboriaud, F.; Ehrhardt, J.-J. Effects of Different Crystal Faces on the Surface Charge of Colloidal Goethite (α-FeOOH) Particles: an Experimental and Modeling Study. *Geochim. Cosmochim. Acta* **2003**, *67*, 967–983.

(41) Kozin, P. A.; Boily, J.-F. Mineral Surface Charge Development in Mixed Electrolyte Solutions. *J. Colloid Interface Sci.* **2014**, *418*, 246–253.

(42) Philpott, M. R.; Glosli, J. N.; Zhu, S.-B. Molecular dynamics simulation of adsorption in electric double layers. *Surf. Sci.* **1995**, *335*, 422–431.

(43) Spohr, E. Computer Simulation of the Structure of the Electrochemical Double Layer. *J. Electroanal. Chem.* **1998**, *450*, 327–334.

(44) Wieckowski, A., Ed. *Interfacial Electrochemistry. Theory, Experiment, and Application*; Marcel Dekker: New York, 1999.

(45) Zarzycki, P.; Kerisit, S.; Rosso, K. M. Molecular Dynamics Study of the Electrical Double Layer at Silver Chloride/Electrolyte Interfaces. *J. Phys. Chem. C* **2010**, *114*, 8905–8916.

(46) Zarzycki, P.; Rosso, K. M. Molecular Dynamics Simulation of the AgCl/Electrolyte Interfacial Capacity. *J. Phys. Chem. C* **2010**, *114*, 10019–10026.

(47) Kerisit, S.; Zarzycki, P.; Rosso, K. M. Computational Molecular Simulation of the Oxidative Adsorption of Ferrous Iron at the Hematite (001)–Water Interface. *J. Phys. Chem. C* **2015**, *119*, 9242–9252.

(48) Rosso, K. M.; Dupuis, M. Electron Transfer in Environmental Systems: a Frontier for Theoretical Chemistry. *Theor. Chem. Acc.* **2005**, *116*, 124–136.

(49) Rosso, K. M.; Smith, D. M. A.; Dupuis, M. An Ab Initio Model of Electron Transport in Hematite (α-Fe_2O_3) Basal Planes. *J. Chem. Phys.* **2003**, *118*, 6455.

(50) Iordanova, N.; Dupuis, M.; Rosso, K. M. Charge Transport in Metal Oxides: A Theoretical Study of Hematite α-Fe_2O_3. *J. Chem. Phys.* **2005**, *122*, 144305.

(51) Marcus, R. A. Electron Transfer Reactions in Chemistry. Theory and Experiment. *Rev. Mod. Phys.* **1993**, *65*, 599–610.

(52) Warshel, A.; Hwang, J. K. Simulation of the Dynamics of Electron Transfer Reactions in Polar Solvents: Semiclassical Trajectories and Dispersed Polaron Approaches. *J. Chem. Phys.* **1986**, *84*, 4938–4957.

(53) Hwang, J. K.; Warshel, A. Microscopic Examination of Free-Energy Relationships for Electron Transfer in Polar Solvents. *J. Am. Chem. Soc.* **1987**, *109*, 715–720.

(54) King, G.; Warshel, A. Investigation of the Free Energy Functions for Electron Transfer reactions. *J. Chem. Phys.* **1990**, *93*, 8682–8692.

(55) Kuharski, R. A.; Bader, J. S.; Chandler, D.; Sprik, M.; Klein, M. L.; Impey, R. W. Molecular Model for Aqueous Ferrous–Ferric electron transfer. *J. Chem. Phys.* **1988**, *89*, 3248–3257.

(56) Pashley, R. M.; Israelachvili, J. N. Molecular Layering of Water in Thin Films Between Mica Surfaces and Its Relation to Hydration Forces. *J. Colloid Interface Sci.* **1984**, *101*, 511–523.

(57) Israelachvili, J.; Wennerström, H. Role of Hydration and Water Structure in Biological and Colloidal Interactions. *Nature* **1996**, *379*, 219–225.

(58) Israelachvili, J. *Intermolecular and Surface Forces*; Academic Press: Amsterdam, 2011.

(59) May, V.; Kühn, O. *Charge and Energy Transfer Dynamics in Molecular Systems*, 3rd ed.; Wiley-VCH: Weinheim, 2011.

(60) Charlton, S. R.; Parkhurst, D. L. Modules Based on the Geochemical Model PHREEQC for Use in Scripting and Programming Languages. *Comput. Geosci.* **2011**, *37*, 1653–1663.

TOC Graphic

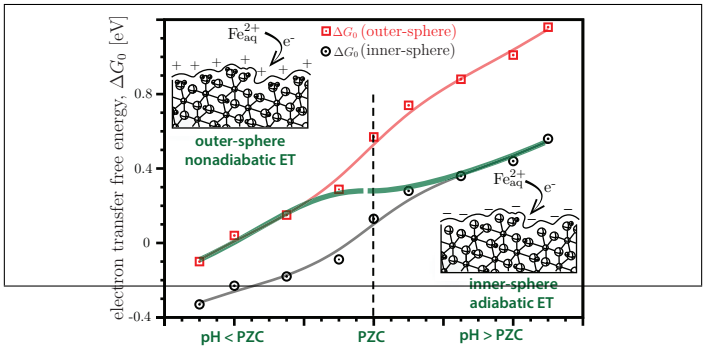
electron transfer free energy, ΔG_0 [eV]
0.8
0.4
0
-0.4
ΔG_0 (outer-sphere)
ΔG_0 (inner-sphere)
Fe^{2+}_{aq}
e^-
outer-sphere
nonadiabatic ET
Fe^{2+}_{aq}
e^-
inner-sphere
adiabatic ET
pH < PZC
PZC
pH > PZC